World Conference on
Timber Engineering
Oslo 2023

NUMERICAL AND EXPERIMENTAL INVESTIGATIONS ON THE STRESS STATE OF CLT-PLATES NEAR CONCENTRATED LOADS

Heinz Wimmer[1], Christoph Huber[2], Robert Eder[3]

ABSTRACT: Cross laminated timber (CLT), as a structural plate-like timber product has been successfully established in civil engineering practice as a load bearing product for walls, floor and roof elements. In a bending situation with transverse shear the cross section does not remain in a plane form due to the strong flexibility of crossing layers. The deformed cross section shows a significant warping which follows a zigzag pattern that influences the stress state. Comparative studies are worked out to investigate the efficiency of two different structural theories. It turned out, that the traditionally used First Order Shear Deformation Theory (FSDT) does not reflect satisfactorily the local stress state near concentrated loads. It is demonstrated that the relatively new Refined Zigzag Theory (RZT) is much better able to represent the stresses in different layers of CLT-plates in such a case. In particular, the rolling shear stress and the maximum bending stress will be strongly underestimated by FSDT, while RZT will provide accurate results. This finding was confirmed by alternative analysis with high-resolution FE continuum elements and by experimental tests using linear strain gauges and a digital image correlation system (DIC) to record the deformations in the area of interest.

KEYWORDS: Cross Laminated Timber, First Order Shear Deformation Theory, Refined Zigzag Theory, Stress state, Rolling shear stress, Concentrated load, Digital image correlation (DIC)

[1] Heinz Wimmer, MPT Engineering GmbH A-4221 Steyregg, Austria, Carinthia University of Applied Sciences, 9800 Spittal /Drau and Upper Austria University of Applied Sciences, 4600 Wels, h.wimmer@fh-kaernten.at
[2] Christoph Huber, KASTNER ZT-GmbH (Civil Engineering), A-9020 Klagenfurt, Austria, c.huber@fh-kaernten.at
[3] Robert Eder, Poltnigg & Klammer ZT-GmbH (Civil Engineering), A-9800 Spittal/Drau, Austria, r.eder@pundk.at

https://doi.org/10.52202/069179-0334

1 INTRODUCTION

Cross laminated timber (CLT), applied as structural plate-like products has revolutionized timber construction for many years. The worldwide production volume is still increasing [1]. For floor systems, single-span strips are predominantly used, characterized by bending with uniaxial load transfer. For the analysis of these types of structural elements many methods exist. A well-known procedure is the Gamma-method [2], originally developed for composite beams with interlayer slip by Möhler [3], which can be modified for applications of CLT. The Shear Analogy (SA) method introduced by Kreuzinger [4] and worked out by Scholz [5,6] provides more capability concerning the local stress state. For beams and plates, the First Order Shear Deformation Theory (FSDT) [7,8] can be used when an appropriate shear correction factor is installed. For multi-span systems as well as for systems with concentrated loads most of the above-mentioned analysis tools are not sufficient to accurately predict the structural behavior, especially the local stress state. In these cases, a higher order plate theory which considers the specific warping phenomenon should be applied. While elaborate 3D analysis is indicated in cases of ultimate load determinations and predictions of damage histories [9], it is useful to resort to structural theories for everyday design tasks. The latter are less complex and easier to handle. In the wide field of theories of composite laminated structures, the following groups are distinguished: Equivalent single layer theories (ESL) [10], Layer-wise theories (LW) [11] and Zigzag Theories [12]. ESL models provide poor results of local variables when employed to highly heterogeneous laminates. The abrupt change of the mechanical properties between layers leads to a change in slope of the in-plane displacements. LW-theories, wherein kinematic assumptions are made for each layer, can reproduce these kinks very well, but the numerical effort increases with the number of plies involved. A good compromise between computational cost and accuracy is offered by the Zigzag models.

The Refined Zigzag Theory (RZT) [13] is an efficient structural theory based on the well-known First Order Shear Deformation Theory, enhanced by local kinematic terms, which allow for the particular attention of warping that arises in the cross section due to shear-elastic layers. The great accuracy of this approach was assessed by comparison with 2D and 3D analytical solutions and 2D-FE solutions as well [13,14]. In a recently published paper, the application of RZT to uniaxial spanned CLT-plates and other shear elastic timber structures like timber-concrete composite beams and timber beams with discrete shear dowels is demonstrated [15]. For single span beams with uniformly distributed loads, there is no significant difference in stress state between FSDT and RZT. In continuous beams and/or when concentrated loads are applied, there are considerable deviations that can no longer be ignored. The Refined Zigzag Theory can work out the qualitative differences that arise from the constrained warping deformations, while FSDT shows an unvarying stress pattern along the whole beam.

2 REFINED ZIGZAG THEORY

The Refined Zigzag Theory was founded in 2010 by Alexander Tessler (NASA) and co-workers from Politecnico di Torino [13]. Since that time many papers have been published, see e.g. references [16–19], showing the tremendous capability of this approach.

2.1 PLATE KINEMATICS

The plate is referred to a Cartesian coordinate system $(\boldsymbol{x}_\beta, z,\ \beta = 1,2)$ (Figure 1). Its thickness h consists of N completely bonded orthotropic layers. The normal surface load $q_z\ (\boldsymbol{x}_\beta)$ is acting on the mid-plane in the positive z-direction. The kinematic field in classical RZT-plate theory is written as

$$\begin{aligned} \boldsymbol{u}_\alpha^{(k)}(\boldsymbol{x}_\beta, z) &= \boldsymbol{u}_\alpha(\boldsymbol{x}_\beta) + z.\theta_\alpha(\boldsymbol{x}_\beta) + \phi_{\alpha\rho}^{(k)}(z).\psi_\alpha(\boldsymbol{x}_\beta) \\ u_z^{(k)}\ (\boldsymbol{x}_\beta, z) &= w(\boldsymbol{x}_\beta) \end{aligned} \quad (1)$$

$\boldsymbol{u}_\alpha^{(k)}(\alpha, \rho = 1,2)$ denote the in-plane displacements, $u_z^{(k)}$ the transversal deflection of the k-th layer. $\boldsymbol{u}_\alpha,\ w,\ \theta_\alpha$ represent the displacements of the mid-plane and the rotations of cross sections respectively. $\phi_{\alpha\rho}^{(k)}$ are the layer-wise linear zigzag functions (Figure 2), which are only dependent of the layer setup and the transversal shear moduli. Finally, ψ_α mean the zigzag rotations which are the two additional degrees of kinematic freedom, by which the warping of the cross section will be controlled. Transverse normal deformation (thickness stretching) is neglected. For angle-ply layers, additional coupling terms $\phi_{12}^{(k)}$ and $\phi_{21}^{(k)}$ should be used in the kinematic equations [20]. With these enhanced kinematic terms also diagonal laminated timber plates (DLT) [21] can be treated.

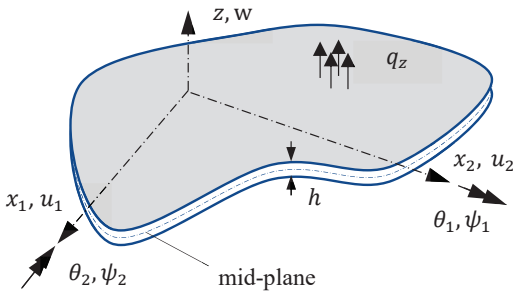

Figure 1: *General plate notation*

Using Green-Lagrange strain-displacement relations with limitation to moderate rotations (von Karman terms) we obtain for the in-plane strains (index p) of a laminated composite plate

https://doi.org/10.52202/069179-0334

$$\boldsymbol{E}_p^{(k)} = \boldsymbol{E}^{(m)} + z.\boldsymbol{E}^{(b)} + \boldsymbol{\Phi}_p^{(k)}(z)\boldsymbol{E}^{(\phi)} \qquad (2)$$

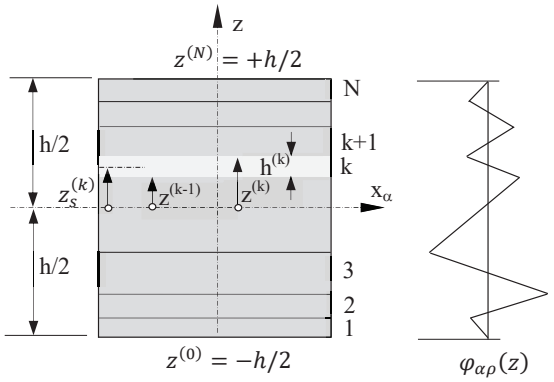

Figure 2: *General layer notation and zigzag function*

Split into the membrane part, the bending part and the zigzag part and with the abbreviation $(.)_{,\alpha} = \frac{\partial}{\partial x_\alpha}$ it follows

$$\boldsymbol{E}^{(m)} = \begin{Bmatrix} u_{,1} + \frac{1}{2}w_{,1}.w_{,1} \\ v_{,2} + \frac{1}{2}w_{,2}.w_{,2} \\ u_{,2} + v_{,1} + w_{,1}.w_{,2} \end{Bmatrix} \qquad (3a)$$

$$\boldsymbol{E}^{(b)} = \begin{Bmatrix} \theta_{1,1} \\ \theta_{2,2} \\ \theta_{1,2} + \theta_{2,1} \end{Bmatrix} \qquad \boldsymbol{E}^{(\phi)} = \begin{Bmatrix} \psi_{1,1} \\ \psi_{2,2} \\ \psi_{1,2} \\ \psi_{2,1} \end{Bmatrix} \qquad (3b, c)$$

$$\boldsymbol{\Phi}_p^{(k)}(z) = \begin{bmatrix} \phi_{11}^{(k)} & 0 & 0 & \phi_{12}^{(k)} \\ 0 & \phi_{22}^{(k)} & \phi_{21}^{(k)} & 0 \\ \phi_{21}^{(k)} & \phi_{12}^{(k)} & \phi_{11}^{(k)} & \phi_{22}^{(k)} \end{bmatrix} \qquad (4)$$

The transverse shear strains (index t) is given by

$$\boldsymbol{E}_t^{(k)} = \boldsymbol{E}_t^{(0)} + \boldsymbol{\Phi}_{t,z}^{(k)}(z)\boldsymbol{\psi} = \boldsymbol{E}_t^{(0)} + \boldsymbol{\beta}^{(k)}\boldsymbol{\psi} \qquad (5)$$

It can be split up into a constant averaged shear part and layer-dependent part

$$\boldsymbol{E}_t^{(0)} = \boldsymbol{\gamma}_t^{(0)} = \begin{Bmatrix} \gamma_1^{(0)} \\ \gamma_2^{(0)} \end{Bmatrix} = \begin{Bmatrix} w_{,1} + \theta_1 \\ w_{,2} + \theta_2 \end{Bmatrix} \quad \boldsymbol{\psi} = \begin{Bmatrix} \psi_1 \\ \psi_2 \end{Bmatrix} \qquad (6a, b)$$

$$\boldsymbol{\Phi}_t^{(k)} = \begin{bmatrix} \phi_{11}^{(k)} & \phi_{12}^{(k)} \\ \phi_{21}^{(k)} & \phi_{22}^{(k)} \end{bmatrix} \qquad \boldsymbol{\beta}^{(k)} = \frac{\partial}{\partial z}\boldsymbol{\Phi}_t^{(k)} = \begin{bmatrix} \beta_{11}^{(k)} & \beta_{12}^{(k)} \\ \beta_{21}^{(k)} & \beta_{22}^{(k)} \end{bmatrix} \qquad (7a, b)$$

Since the zigzag functions $\phi_{\alpha\rho}^{(k)}$ are chosen as layer-wise linear functions, the $\beta_{\alpha\rho}^{(k)}$ functions which influence the shear stresses (see Equation (7) and (8)) are constant for each layer, leading to mean values of shear stress. This means that in the classical RZT the local equilibrium condition of shear stresses at the interlayer and on top and bottom is violated, just like in FSDT. It has been shown by Tessler and co-workers [22,23], that by the application of Reissner´s mixed variational principle (RZT^m) this deficiency can be eliminated.

According to the assumption of plane stress state ($S_{33} = 0$) these strains are connected by the elastic Hookean law with the corresponding second Piola-Kirchhoff stress quantities

$$\boldsymbol{S}_p^{(k)} = \begin{Bmatrix} S_{11} \\ S_{22} \\ S_{12} \end{Bmatrix}^{(k)} = \overline{\boldsymbol{Q}}_p\boldsymbol{E}_p^{(k)} \qquad \boldsymbol{S}_t^{(k)} = \begin{Bmatrix} S_{13} \\ S_{23} \end{Bmatrix}^{(k)} = \overline{\boldsymbol{Q}}_t\boldsymbol{\gamma}_t^{(k)} \qquad (8a, b)$$

The matrices $\overline{\boldsymbol{Q}}$ contain the transformed plane stress reduced stiffness coefficients [7,8].

$$\overline{\boldsymbol{Q}}_p^{(k)} = \begin{bmatrix} \bar{Q}_{11} & \bar{Q}_{12} & \bar{Q}_{16} \\ \bar{Q}_{12} & \bar{Q}_{22} & \bar{Q}_{26} \\ \bar{Q}_{16} & \bar{Q}_{26} & \bar{Q}_{66} \end{bmatrix}^{(k)} \qquad \overline{\boldsymbol{Q}}_t^{(k)} = \begin{bmatrix} \bar{Q}_{44} & \bar{Q}_{45} \\ \bar{Q}_{45} & \bar{Q}_{55} \end{bmatrix}^{(k)} \qquad (9a, b)$$

To establish the discretized problem the principle of virtual work says

$$\delta W_{int} - \delta W_{ext} = 0 \qquad (10)$$

In detail the virtual work done by the inner forces reads

$$\delta W_{int} = \int \delta\boldsymbol{E}_p^T\boldsymbol{S}_p\, dV + \int \delta\boldsymbol{E}_t^T\boldsymbol{S}_t\, dV \qquad (11)$$

Integration over the thickness of the first part leads to

$$\delta W_{int} = \int \delta\boldsymbol{E}_p^T\boldsymbol{R}_p\, dA + \int \delta\boldsymbol{E}_t^T\boldsymbol{R}_t\, dA \qquad (12)$$

with the second Piola-Kirchoff-stress resultants

$$\boldsymbol{R}_p = \begin{Bmatrix} \boldsymbol{N} \\ \boldsymbol{M} \\ \boldsymbol{M}_\phi \end{Bmatrix} \qquad \boldsymbol{R}_t = \begin{Bmatrix} \boldsymbol{T} \\ \boldsymbol{T}_\phi \end{Bmatrix} \qquad (13)$$

2.2 CONSTITUTIVE RELATIONS OF THE WHOLE LAMINATE

From the above equations we get in summary the special plate constitutive equation. In full we have 14 strain components and stress resultants

$$\boldsymbol{R} = \begin{Bmatrix} \boldsymbol{R}_p \\ \boldsymbol{R}_t \end{Bmatrix} = \boldsymbol{C}\boldsymbol{E} = \boldsymbol{C}\begin{Bmatrix} \boldsymbol{E}^{(m)} \\ \boldsymbol{E}^{(b)} \\ \boldsymbol{E}^{(\phi)} \\ \boldsymbol{\gamma}^{(0)} \\ \boldsymbol{\psi} \end{Bmatrix} \qquad (14)$$

In detail we have

$$\begin{Bmatrix} \boldsymbol{N} \\ \boldsymbol{M} \\ \boldsymbol{M}^{(\phi)} \\ \boldsymbol{T} \\ \boldsymbol{T}^{(\phi)} \end{Bmatrix} = \begin{bmatrix} \boldsymbol{A} & \boldsymbol{B} & \boldsymbol{A}^{\boldsymbol{\phi}} & 0 & \boldsymbol{0} \\ \boldsymbol{B}^{\boldsymbol{T}} & \boldsymbol{D} & \boldsymbol{B}^{\phi} & 0 & 0 \\ \boldsymbol{A}^{\phi T} & \boldsymbol{B}^{\phi T} & \boldsymbol{D}^{\phi} & 0 & 0 \\ 0 & 0 & 0 & \boldsymbol{A}_t & \boldsymbol{B}_t^{(\phi)} \\ 0 & 0 & 0 & \boldsymbol{B}_t^{(\phi)T} & \boldsymbol{D}_t^{(\phi)} \end{bmatrix} \begin{Bmatrix} \boldsymbol{E}^{(m)} \\ \boldsymbol{E}^{(b)} \\ \boldsymbol{E}^{(\phi)} \\ \boldsymbol{\gamma}^{(0)} \\ \boldsymbol{\psi} \end{Bmatrix} \qquad (15)$$

https://doi.org/10.52202/069179-0334

The constitutive matrix **C** is built up by the following sub matrices, emerging from the integration of the weighted, reduced elastic stiffness coefficients over the thickness.

$$(\boldsymbol{A},\boldsymbol{B},\boldsymbol{D}) \equiv \int_{-\frac{h}{2}}^{+\frac{h}{2}} (1,z,z^2)\,\overline{\boldsymbol{Q}}_p^{(k)}\,dz \tag{16a}$$

$$\left(\boldsymbol{A}^{\boldsymbol{\phi}},\boldsymbol{B}^{\boldsymbol{\phi}},\boldsymbol{D}^{\boldsymbol{\phi}}\right) \equiv \int_{-\frac{h}{2}}^{+\frac{h}{2}} \left(1,z,\boldsymbol{\Phi}_p^{(k)T}\right)\overline{\boldsymbol{Q}}_p^{(k)}\boldsymbol{\Phi}_p^{(k)}\,dz \tag{16b}$$

$$\left(\boldsymbol{A}_t,\boldsymbol{B}_t^{(\phi)}\right) \equiv \int_{-\frac{h}{2}}^{+\frac{h}{2}} \left(1,\boldsymbol{\beta}^{(k)}\right)\overline{\boldsymbol{Q}}_t^{(k)}\,dz \tag{16c}$$

$$\boldsymbol{D}_t^{(\phi)} \equiv \int_{-\frac{h}{2}}^{+\frac{h}{2}} \boldsymbol{\beta}^{(k)T}\overline{\boldsymbol{Q}}_t^{(k)}\boldsymbol{\beta}^{(k)}\,dz \tag{16d}$$

The enhanced zigzag functions are established by layer-wise integration of the $\boldsymbol{\beta}^{(k)}$ functions. The latter are derived from a relaxed continuity condition of shear stresses at the interlayer and the assumption that the zigzag functions vanish at the top and bottom surfaces of the plate, see Sorrenti et al. [20]. The model allows for a piecewise constant distribution of transverse shear stresses that is accurate in an average sense.

The corresponding relations for the laminated beam in the x-z-plane can be found in [24]:

$$\begin{Bmatrix} N_x \\ M_x \\ M_\phi \end{Bmatrix} \equiv \begin{bmatrix} A_{11} & B_{12} & B_{13} \\ B_{12} & D_{11} & D_{12} \\ B_{13} & D_{12} & D_{22} \end{bmatrix} \begin{Bmatrix} u_{,x} \\ \theta_{,x} \\ \psi_{,x} \end{Bmatrix} \tag{17}$$

The stiffness coefficients are defined as

$$[A_{11},B_{12},D_{11}] \equiv \int_A C_{11}^{(k)}[1,z,z^2]b^{(k)}(z)\,dz \tag{18a}$$

$$[B_{13},D_{12},D_{22}] \equiv \int_A C_{11}^{(k)}\phi^{(k)}\left[1,z,\phi^{(k)}\right]b^{(k)}(z)\,dz \tag{18b}$$

which can be calculated analytically. For a beam in plane strain in width direction b, $C_{11}^{(k)} = E_x^{(k)}/\left(1-\nu_{xy}^{(k)}\nu_{yx}^{(k)}\right)$ and for beam in plane stress $C_{11}^{(k)} = E_x^{(k)}$, where $E_x^{(k)}$ is the Young´s modulus of the *k*-th layer in axial direction *x* and $\nu_{xy}^{(k)}$, $\nu_{yx}^{(k)}$ are the Poisson´s ratios. Beams with unequal ply width can also be analyzed when a modification of the shear modulus $G_{xz}^{(k)}$ is performed [15].

3 FINITE ELEMENTS

This section summarizes the main finite element developments of the last ten years based on refined zigzag kinematics.

3.1 BEAM ELEMENT

The first numerical implementation was presented by Gherlone et al. [25] using a C^0-element based on an anisoparametric interpolation scheme originally proposed by Tessler and Dong [26]. Di Sciuva et al. [27] has given an extension to a class of higher-order elements. Wimmer et al. [24] provided explicit representations for the stiffness, the geometric stiffness and the mass matrix and an exact version of the stiffness matrix has been worked out in [28]. Flores et al. [29] reflected some limitations of RZT when modelling delamination. Kefal and coworkers [30] presented an iso-geometric beam element based on RZT^m.

There are only a few papers that explicitly report on the experimental verification of RZT. Experimental evaluations of the static and dynamic response of sandwich beams are presented by Iurlaro et al. [31,32]. Buckling test are performed and reported by Ascione et al. [33].

It should be pointed out, that in FSDT beam analysis the shear stress pattern in the cross section does not vary along the beam axis, while in RZT it happens due to the additional kinematic degree of freedom ψ, as can be seen from Equation (5). The mean shear stress obtained by the corresponding constitutive equation of FSDT therefore underestimates the real value dramatically (see Figure 5). For this reason, the shear stress distribution is usually calculated by integrating the local equilibrium equation (Cauchy´s equation) [34]. An analogous procedure derived by Tessler [22] leads to

$$\begin{aligned}\tau_{xz}^{(k)}(x,z) = {} & \theta_{,xx}(x)\left[\frac{B_{12}}{A_{11}}\tau_u^{(k)}(z) - \tau_\theta^{(k)}(z)\right] + \\ & + \psi_{,xx}(x)\left[\frac{B_{13}}{A_{11}}\tau_u^{(k)}(z) - \tau_\psi^{(k)}(z)\right]\end{aligned} \tag{19}$$

with the integrals

$$\tau_u^{(k)}(z) \equiv \int_{-h/2}^{z} C_{11}^{(k)}\,d\bar{z} \tag{20a}$$

$$\tau_\theta^{(k)}(z) \equiv \int_{-h/2}^{z} \bar{z}\,C_{11}^{(k)}\,d\bar{z} \tag{20b}$$

$$\tau_\psi^{(k)}(z) \equiv \int_{-h/2}^{z} \phi^{(k)}(\bar{z})\,C_{11}^{(k)}\,d\bar{z} \tag{20c}$$

In case of shear stresses on the top and bottom side an additional term must be considered. When referring to FSDT all terms associated with ψ are omitted.

3.2 PLATE ELEMENT

A first application for bi-axial plate bending is given by Versino [16], who extended Tessler´s anisoparametric shape functions originally presented in the well-known homogeneous plate element MIN3 to RZT-kinematics. Recently Sorrenti et al. [18] reported a robust quadrilateral version which achieves reliable results even in the ultra-thin range. Wimmer et al. [17] has demonstrated the advantages that can be reaped when the so-called smoothed finite element technique is employed. Hasim et al. [35] has presented an iso-geometric variant that allows for plates with curvilinear fibers. Wimmer and co-workers [36] has recently shown the extension to buckling and geometrical-nonlinear bending.

4 NUMERICAL RESULTS

Two representative examples are given in this section. As a first example a continuous beam is investigated. In

another example, the biaxial bending state of a CLT strip intermediately supported by a column is treated.

4.1 UNIAXIAL BENDING

A two-span CLT-beam is investigated as a beam model (with RZT and FSDT) and as a 2D-continuum. The cross-section consists of five layers of equal thickness with $h^{(k)} = 0.04$ m.

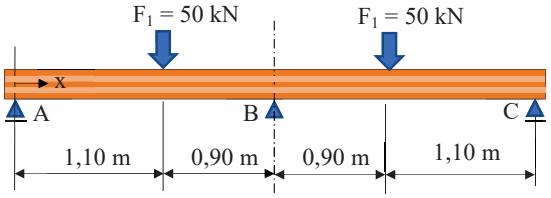

Figure 3: *System of a two-span continuous test beam under concentrated loads (uniaxial bending)*

The single boards are edge-glued. The beam has a width of b = 0.50 m and an overhang of 0.20 m at both ends. Two concentrated loads F_1 = 50 kN act approximately in the middle of the span (Figure 3 and 10). An additional force of ΔF_1 = 1.84 kN was taken into account for the load transmission beam. As the structure is first analyzed as a beam model [24], the forces as well as the support reactions are applied via distributed loads with respect to the axis of the beam. At the force application point, a parabolic line load with amplitude q_F = 243 kN/m is modeled, acting over a length of 0.32 m, while the line load at the intermediate support has an amplitude of q_B = –475.6 kN/m, distributed over a width of 0.24 m, resulting in a reaction force B = 76.1 kN. In the 2D-continuum model the actions are located as uniform pressures on the top and the bottom side of the beam.
The material data for the numerical model were chosen as mean values from component tests of the single boards. To achieve the experimentally determined maximum deflection of w_{max} = 2.85 mm, the rolling shear modulus had to be adjusted concerning the experimental measure-ments (see section 5.3):

$E_x = E_0 = 11600$ MPa, $E_y = E_z = E_{90} = 370$ MPa, $G_{xz} = G_{090} = 560$ MPa, $G_{xz} = G_{yz} = G_{9090} = 120$ MPa.

4.1.1 Longitudinal Stress

The maximum bending stress distribution along the beam is given in Figure 4. It shows the significant influence of the cross sectional warping close to the load transfer zone.
In addition, the structure is modeled with 2D-continuum elements of high resolution (3 rows of solid elements for each layer). The maximum deflection must be corrected for thickness deformation when comparing with the beam solution. The peak values of RZT-beam solution are quite well confirmed by 2D-FE analysis. It should be noted that when using 2D continuum elements, no rotational degree of freedom at the nodes of the interlayer boundaries should be present (or it should be released). Otherwise, the typical kink is numerically cancelled, and the stress state could be locally distorted as a result. The measured values of the linear strain gauges (mean values of three specimens), which are attached to the tensile side of the load application points (Figure 10), impressively confirm the numerical values of the RZT.

4.1.2 Shear Stress

The standard method of RZT and FSDT as well provides only mean values of the shear stresses in each layer. It

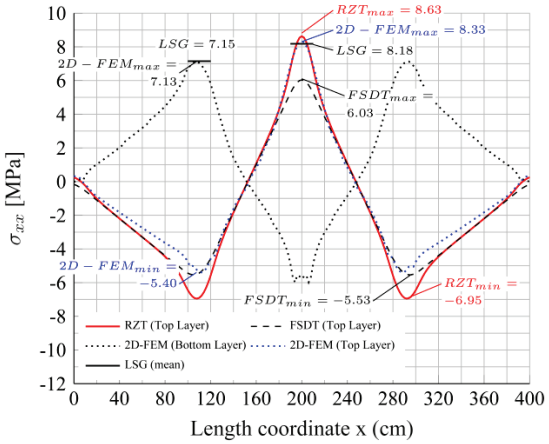

Figure 4: *Maximum bending stress along the axis of a two-span continuous beam for different composite beam theories, from 2D continuum analysis and experimental results.*

turned out that the standard FSDT is not able to reflect the stress state accurately. In particular, the rolling shear stress in the second layer is completely miscalculated qualitatively and quantitatively. It became apparent, that FSDT significantly underestimates the mean values of rolling shear stress (Figure 5) when using the constitutive equation. Figure 6 presents the shear stress distributions $\tau_{xz}(z)$ along several sections (see Figure 10) coming from
different calculation approaches. Figure 6 (upper graph) shows the mean values (FSDTm) recovered from the constitutive equations and the values which result from

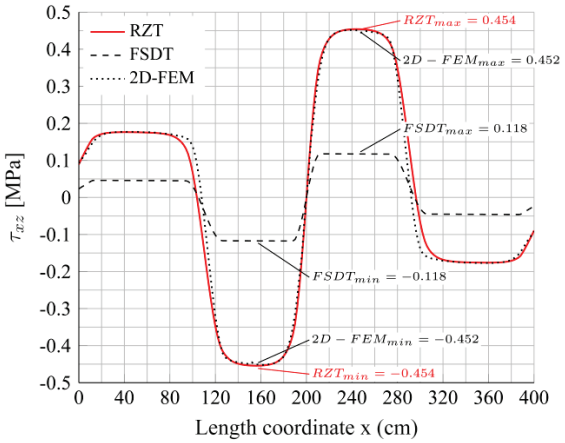

Figure 5: *Rolling shear stress in the second layer along the axis of a two-span continuous beam under concentrated loads for different composite beam theories and 2D continuum analysis.*

https://doi.org/10.52202/069179-0334

integration of Cauchy´s equation (FSDTc, Eq.19, 20). Figure 6 (lower graph) gives the corresponding results for RZT. It is noticeable, that RZT provides accurate values of the rolling shear stress in the second layer even if the constitutive equation is applied. Outside the warping zone, both theories give the same result when the integration technique is applied. In the load transfer zone, the symmetry is lost under the influence of the transverse normal stress σ_{zz}, as can be seen in section 0 - 0, but the maximum shear stress given by the RZT and the integration method reproduces the 2D solution quite well.

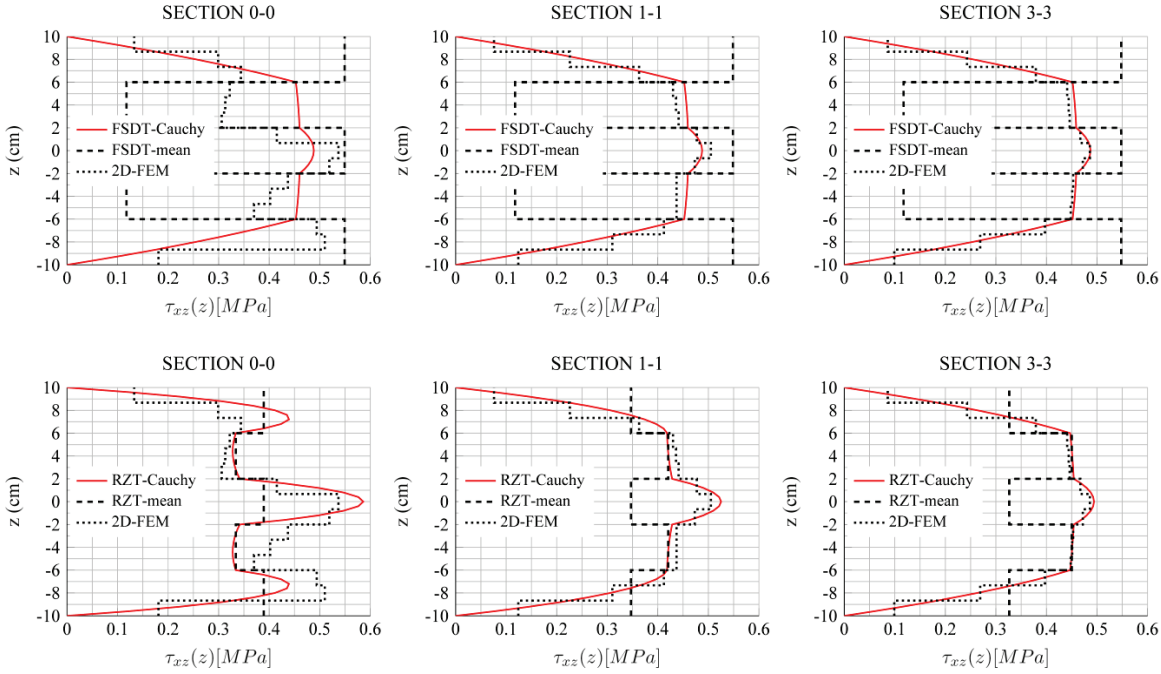

Figure 6: *Shear stress distributions $\tau_{xz}(z)$ (mean values, Cauchy-integrated and unsmoothed 2D-solution) for FSDT (upper graph) and for RZT (bottom graph) along different cross sections*

4.2 BIAXIAL BENDING

A double-symmetric, two-span rectangular CLT-plate (Figure 7) with dimensions 7.80 / 2.40 / 0.20 m, resting on a line support at both ends and a point intermediate bearing (30 x 30 cm) is studied with a plate model [17] considering the above two theories and a 3D continuum model. A quarter of the plate (3.90 / 1.20 m) is modeled and subjected by a constant surface load on the upper side of q_z = -10 kN/m^2. The contact area at the corner (0.15 / 0.15 m) has a subgrade reaction modulus of 3.3 10^6 kN/m^3. The cross section consists of 5 layers, each with equal thickness of 4 cm. The following material parameter were applied:

E_1 = 11500 MPa, $E_2 = E_3$ = 370 MPa, $G_{12} = G_{13}$ = 690 MPa, G_{23} = 50 MPa. ν_{12} = 0.38, ν_{13} = 0.22, ν_{23} = 0.203.

The material axis 1 coincide with the x_1-axis. The layer setup is 0/90/0/90/0°.

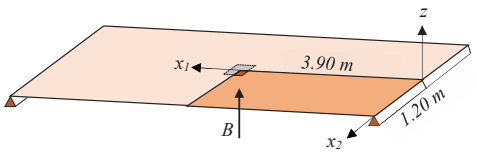

Figure 7: *Biaxial bending of CLT-plate with point intermediate support*

Table 1: *Maximum deflection and bending stresses in the upper two layers of a CLT-plate (symmetry point) under biaxial bending, 3D deflection corrected from thickness compression*

	FSDT	RZT	3D
max w [mm]	5.91	5.18	5.39
max σ_{11} [MPa]	5.68	9.23	9.71
max σ_{22} [MPa]	6.92	10.64	10.98

For comparison the plate is analyzed with the FE-program ABAQUS using more than 40 000 quadratic solids elements of type C3D20. Figure 8 shows the transverse deformation u3 = w and clearly the typical zigzag pattern arising from the heterogeneous cross section under high transverse shear stresses. In Table 1

https://doi.org/10.52202/069179-0334

essential results are presented. Figure 9 gives the through- thickness distribution of stresses at the center point of the whole plate in both directions. It demonstrates the superior accuracy of RZT against FSDT. As with the uniaxial example, it can be seen that FSDT significantly underestimates the maximum bending stresses.

5 EXPERIMENTAL RESULTS

In the following, the experimental configurations as well as the measurement systems for the test beam (see Figure 3) are described. Furthermore, the measured data are analyzed and compared with the results from the numerical analysis.

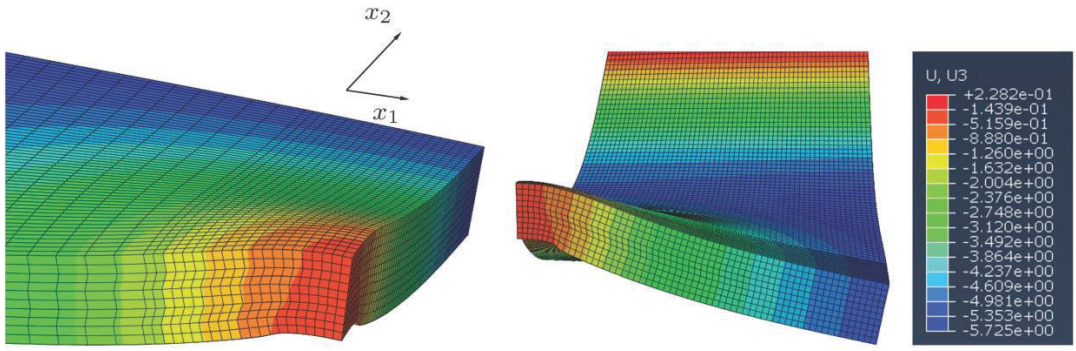

Figure 8: *Warping deformation near the point support along the planes of symmetry with typical zigzag pattern*

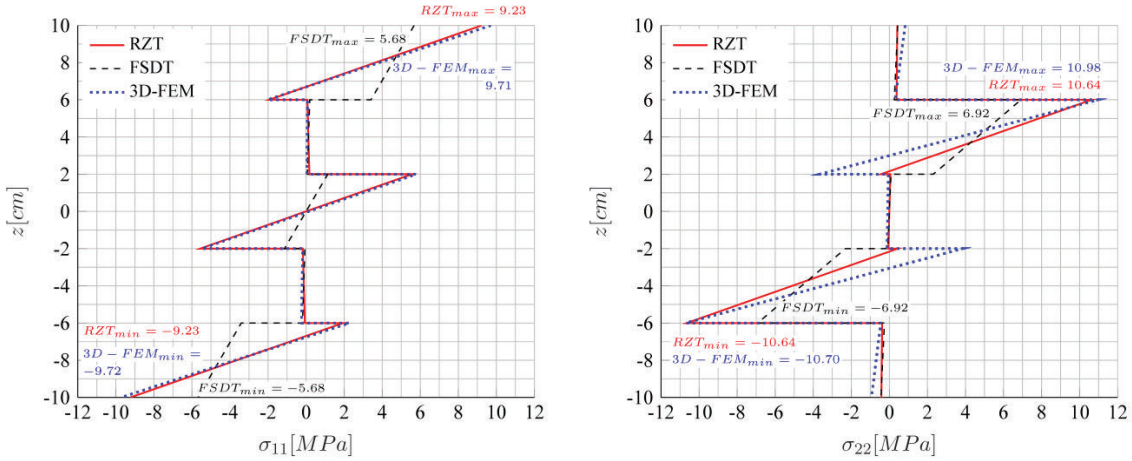

Figure 9: *Bending stresses distribution at the symmetry point by different structural theories*

5.1 EXPERIMENTAL SETUP

Figure 10 shows the experimental setup for the bending test. The hydraulic jack is fixed on a rigid loading frame. The latter is clamped to the rigid floor with anchor bolts. The load is applied via a crossbeam (HEM 280). The two-span beam has three roller supports. For dimensions and loads see section 4.1. The cross section of the test beam has a width of 50 cm.

The shear slenderness at the supports in both bays is a/d = 110/20 = 5.5 and concerning the inner support a/d = 90/20 = 4.5. The test program includes three test specimens. Figure 10 shows the four measurement methods used. A measuring box in the hydraulic jack reported the test load. In the range of the load application as well as above the intermediate support, linear strain gauges (LSG) were responsible for measuring the strains of the top and bottom fiber. To measure the vertical deflection, a displacement sensor was placed under the load application point. A DIC-System is used to detect strains in the area of interest (AOI). The load rate is determined at 0.5 mm/min. for all tests.

https://doi.org/10.52202/069179-0334

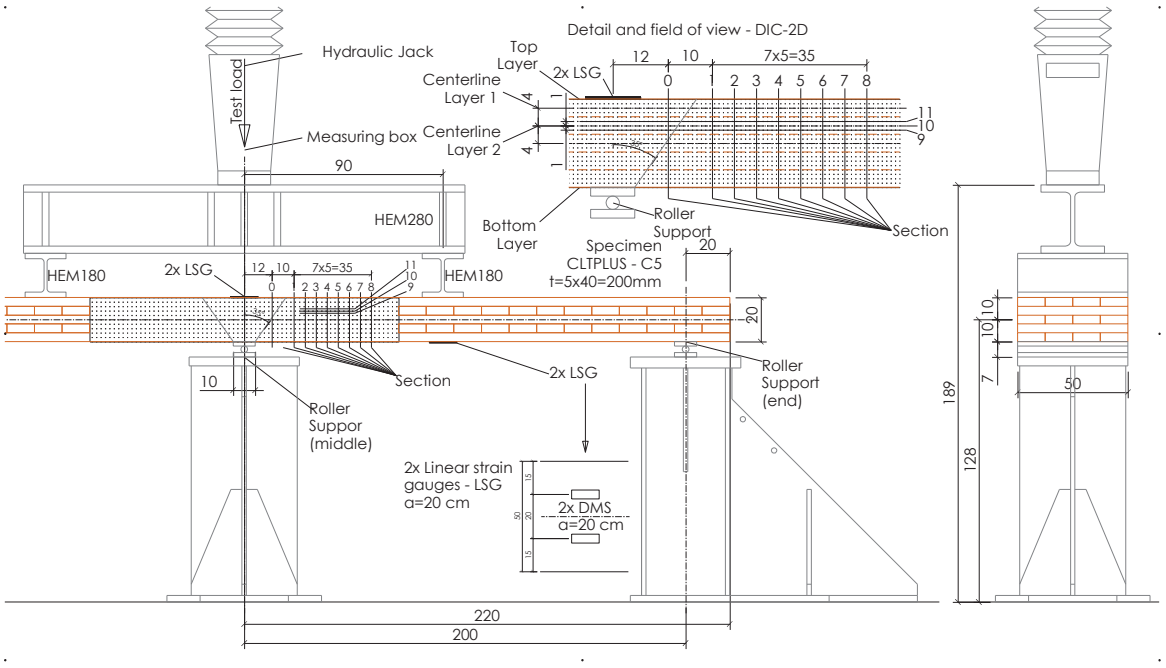

Figure 10: *Experimental setup of a CLT-beam*

5.2 Digital image correlation (DIC)

The DIC-System as an optical, contactless deformation measurement method combines image registration and tracking system for precise 2D measurements to reconstruct the strain state in a structural component. In this study, the DIC-System was used to monitor the strains and deformations near the intermediate support. Just left and right of this support the lateral surface of the beam was speckled randomly and 2D measurement method is employed. The strains and deformations are measured in the area of interest and compared with the numerical results.

5.3 Evaluation of strains

The DIC system provides Green-Lagrange strains. The evaluation of shear angles $\gamma_{xz} = 2\varepsilon_{xz}$ was carried out along vertical sections 0 – 8 (see Figure 10) and showed an unsteady distribution related to the strong inhomogeneity caused by the individual fibers. (Figure 11). Based on these distributions, mean values $\gamma_{xz,m}$ are calculated for each layer. Subsequently they were multiplied layer-wise by those shear moduli G_{xz} that lead to match with the results from 2D-FE analysis which in turn fulfil the equilibrium conditions.

The calibration procedure is performed for all vertical sections marked in Figure 10, separated according to layers, resulting in the following mean values: G_{9090} = 120 MPa, G_{090} = 560 MPa.

A comparison with extensive tests reported in [37] as well as numerical investigations [38] showed good congruence of these values.

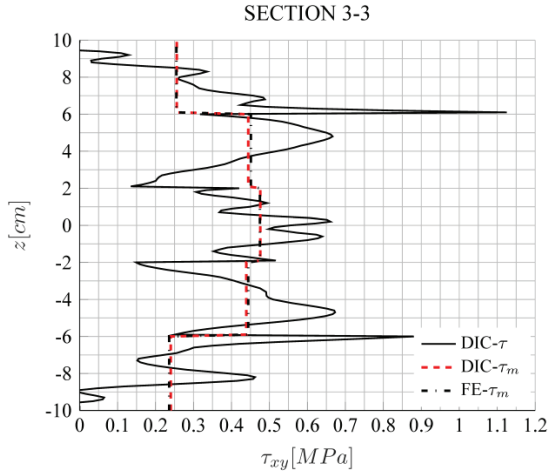

Figure 11: *Shear stress distribution measured by DIC and mean values per layer*

6 ULS-DESIGN

The clearly recognizable stress peaks in the examples shown have a non-negligible influence on the design process. The utilization factor with respect to the axial stresses in the grain direction, which is given in Tables 2, 3 and 4, was evaluated by the formula of Equation (21), where $\sigma_{t/c,0,CLT,d}$ and $f_{t/c,0,CLT,d}$ denote the design values of max/min. stress and strength parallel to the grain for

$$U_{t/c} = \frac{|\sigma_{t/c,0,mean,d}|}{f_{t/c,0,CLT,d}} + \frac{|\sigma_{m,CLT,d}|}{f_{m,CLT,d}} \qquad (21)$$

https://doi.org/10.52202/069179-0334

pure tension (t) or compression (c), respectively. $\sigma_{t/c,mean,d}$ represents the mean value of the linearly varying stress distribution in the uppermost or lowermost layer. The second part $\sigma_{m,CLT,d}$ is given by the nonuniform part of bending stress deviating from the above-mentioned mean value and the bending strength $f_{m,CLT,d}$. For the comparison we refer to the design format of Eurocode 5 and the following material parameters, proposed in [1]: $f_{m,CLT,k}$ = 24 N/mm^2, $f_{c,0,CLT,k}$ = 24 N/mm^2, $f_{t,0,CLT,k}$ = 16 N/mm^2. For the corresponding design values, $k_{mod} = 0.80, \gamma_M = 1.25$ was chosen.

Table 2: *Comparison of utilization factor $U_{c/t}$ concerning axial stresses of example 1 (uniaxial bending) at the intermediate support.*

Layer	z-Pos. [mm]		FSDT [MPa]	RZT [MPa]	Δ %
5/1	±100	$\pm\sigma_{t,0,CLT,d}$	6.03	8.63	43
	±80	$\pm\sigma_{t,0,mean,d}$	4.835	4.525	
		$\pm\sigma_{m,CLT,d}$	1.195	4.105	
5	+100	U_t	0.550	0.709	29
1	-100	U_c	0,393	0,562	43

Table 3: *Comparison of utilization factor $U_{c/t}$ concerning axial stresses of example 2 (symmetry point) in x-direction*

Layer	z-Pos. [mm]		FSDT [MPa]	RZT [MPa]	Δ %
5/1	±100	$\pm\sigma_{t,0,CLT,d}$	5.68	9.23	63
	±80	$\pm\sigma_{t,0,mean,d}$	4.545	3.645	
		$\pm\sigma_{m,CLT,d}$	1.135	5.585	
5	+100	U_t	0.518	0.720	39
1	-100	U_c	0.37	0.601	63

Table 4: *Comparison of utilization factor $U_{c/t}$ concerning axial stresses of example 2 (symmetry point) in y-direction*

Layer	z-Pos. [mm]		FSDT [MPa]	RZT [MPa]	Δ %
4/2	±60	$\pm\sigma_{t,0,CLT,d}$	6.92	10.64	54
	±40	$\pm\sigma_{t,0,mean,d}$	4.62	5.10	
		$\pm\sigma_{m,CLT,d}$	2.31	5.54	
4	+60	U_t	0.601	0.859	43
2	-60	U_c	0.451	0.693	54

7 CONCLUSIONS

Comparative studies on uniaxial and biaxial loaded CLT-plates under concentrated loads have shown the superiority of Refined Zigzag Theory over the traditionally used First Order Shear Deformation Theory. The bending and shear stresses predicted by the RZT are impressively confirmed by numerical comparative calculations with continuum elements and experimental measurements. It could be proven that using the FSDT-based axial stress values leads to an underestimation of the corresponding utilization factor of CLT-plates up to 50 % and more. When applying the FSDT the rolling shear stress must be determined by integration of Cauchy´s equilibrium equation otherwise it is dramatically underestimated. In case of uniaxial bending the RZT already reliably predicts the rolling shear stress in the standard procedure using the constitutive equation. The propagated RZT forms a good compromise in terms of computational effort and achieved accuracy. It does not require a shear correction factor. It represents a consistent extension of the FSDT showing a great similarity to that between Saint Venant's torsion and warping torsion. Since it is the simplest variant among the numerous higher-order shear deformation theories, it should be used as the new standard tool for the analysis of CLT plates and other shear-elastic structures in the everday design process.

ACKNOWLEDGEMENT

This work would not have been possible without the financial and technical support of the following involved parties, the Innovation Voucher - Program of the Austria FFG Funding Service, consultancy firm Poltnigg & Klammer ZT-GmbH & KASTNER ZT-GmbH, Carinthia, Theurl - Timber Structures GmbH and the Baulabor of the Carinthia University of Applied Sciences. Special thanks to Tamas Meszöly and Lukas Kepplinger for their contributions.

REFERENCES

[1] Brandner R., Flatscher G., Ringhofer A., Schickhofer G., Thiel A.: Cross laminated timber (CLT): overview and development. European Journal of Wood and Wood Products 74:331-351, 2016.

[2] EN 1995-1-1, Eurocode 5: Design of timber structures – Part 1-1: Genera–common rules and rules for buildings, 2019.

[3] Möhler K.: Über das Tragverhalten von Biegeträgern und Druckstäben mit zusammengesetzten Quer-schnitten und nachgiebigen Verbindungsmittels, Habilitation TH Karlsruhe (in German), 1956.

[4] Kreuzinger H.: Flächentragwerke, Platten, Scheiben und Schalen, Berechnungsmethoden und Beispiele. In: Brücken aus Holz. Informationsdienst Holz, Arbeitsgemeinschaft Holz e.V. Düsseldorf (in German), 1999.

[5] Scholz A.: Structural analysis of wooden plate structures. 4th International PhD Symposium in Civil Engineering, Munich, 2002.

[6] Scholz A.: Ein Beitrag zur Berechnung von Flächentragwerken aus Holz. PhD thesis Technische Universität München (in German), 2004.

[7] Altenbach H., Altenbach J., Kissing W.: Mechanics of Composite Structural Elements. Springer Berlin 2004.

[8] Reddy J.N.: Mechanics of laminated composite plates and shells. CRC Press, London, 2004.

https://doi.org/10.52202/069179-0334

[9] Hochreiner G., Füssl J., Eberhardsteiner J.: Cross-laminated timber plates subjected to concentrated loading - Experimental identification of failure mechanisms. Strain, 50:68-81, 2013.
[10] Abrate S., Di Sciuva M.: Equivalent single layer theories for composite and sandwich structures: A review. Compos. Struct., 179:482-494, 2017.
[11] Liew K.M., Pan Z.Z., Zhang L.W.: An overview of layerwise theories for composite laminates and structures: Development, numerical implementation and application. Comp. Struct., 216:240-259, 2019.
[12] Icardi U., Sola F.: Assessment of recent zig-zag theories for laminated and sandwich structures. Composites Part B, 97:26-52, 2016.
[13] Tessler A., Di Sciuva M., Gherlone M.: A consistent refinement of first-order shear deformation theory for laminated composite and sandwich plates using improved zigzag kinematics. J. Mech. Mat. Struct., 5:341–367, 2010.
[14] Iurlaro L., Gherlone M., Di Sciuva M., Tessler A.: Assessment of the refined zigzag theory for bending, vibration, and buckling of sandwich plates: a comparative study of different theories. Compos. Struct., 106:777–792, 2013.
[15] Wimmer H., Hochhauser W., Nachbagauer K.: Refined Zigzag Theory: an appropriate tool for the analysis of CLT-plates and other shear-elastic timber structures. European Journal of Wood and Wood Products. https://doi.org/10.1007/s00107-020-01586-x, 2020.
[16] Versino D., Gherlone M., Mattone M., Di Sciuva M., Tessler A.: C0 triangular elements based on the Refined Zigzag Theory for multilayer composite and sandwich plates. Composites Part B, 44:218-230, 2013.
[17] Wimmer H., Celigoj Ch.: An edge-based smoothed three-node composite plate element with refined zigzag kinematics. Compos. Struct., 274, 114204, 2021.
[18] Sorrenti M., Di Sciuva M., Tessler A.: A robust four-node quadrilateral element for laminated composite and sandwich plates based on refined zigzag theory. Computers & Structures, 242, 106369, 2021.
[19] Gherlone M., Versino D., Zarra V.: Multilayered triangular and quadrilateral flat shell elements based on the Refined Zigzag Theory. Composite Structures, 233, 111629, 2020.
[20] Sorrenti M., Di Sciuva M.: An Enhancement of Warping Shear Functions of Refined Zigzag Theory. J. Appl. Mech., 88, 084501-1, 2021.
[21] Arnold M., Dietsch Ph., Maderebner R., Winter S.: Diagonal laminated timber — Experimental, analytical, and numerical studies on the torsional stiffness. Construction and Building Materials, 322, doi.org/10.1016/j.conbuildmat.2022.126455, 2022.
[22] Tessler A.: Refined zigzag theory for homogeneous, laminated composite, and sandwich beams derived from Reissner´s mixed variational principle. Meccanica, 50:2621-2648, 2015.
[23] Groh R.M.J., Tessler A.: Computationally efficient beam elements for accurate stresses in sandwich laminates and laminated composites with delaminations. Comp. Methods Appl. Mech. Engrg., 320:369-395, 2017.
[24] Wimmer H., Gherlone M., Explicit matrices for a composite beam-column with refined zigzag kinematics. Acta Mech., 228:2107–2117, 2017.
[25] Gherlone M., Tessler A., Di Sciuva M.: C0 beam elements based on Refined Zigzag Theory for multilayered composite and sandwich laminates. Composite Structures, 93:2882-2894, 2011.
[26] Tessler A., Dong S.B.: On a hierarchy of conforming Timoshenko beam elements. Computers & Structures, 14:335-344, 1981.
[27] Di Sciuva M., Gherlone M. Iurlaro L., Tessler A.: A class of higher order C0 composite and sandwich bean elements based on the Refined Zigzag Theory. Composite Structures, 132:784-803, 2015.
[28] Wimmer H., Nachbagauer K.: Exact transfer- and stiffness matrix for the composite beam-column with Refined Zigzag Kinematics. Composite Structures, 189:700-706, 2018.
[29] Flores G.F., Oller S., Nallim L.G.: On the analysis of non-homogeneuos laminates using the refined zigzag theory. Composite Structures, 204:791-802, 2018.
[30] Kefal A., Hasim K.A., Yildiz M.: A novel isogeometric beam element based on mixed form of refined zigzag theory for thick sandwich and multilayered composite beams. Composites Part B, 167:100-121, 2019.
[31] Iurlaro L., Gherlone M., Mattone M., Di Sciuva M.: Experimental assessment of the Refined Zigzag Theory for the static bending analysis of sandwich beams. J. Sandwich Structures and Materials, 20:86-105, 2018.
[32] Iurlaro L., Ascione A., Gherlone M., Mattone M., Di Sciuva M.: Free vibration analysis of sandwich beams using the refined zigzag theory: an experimental assessment. Mecchanica, 50:2525-2535, 2015.
[33] Ascione A., Orifici A.C., Gherlone M.: Experimental and Numerical Investigations of the Refined Zigzag Theory for the Accurate Buckling Analysis of Highly Heterogeneous Sandwich Beams. Int. J. Struct. Stab. Dyn., 20 (7): 2050078, 2020.
[34] Rolfes R., Rohwer K.: Improved transverse shear stresses in composite finite element based on first order shear deformation theory. Int. J. Num. Meth. Eng., 40:51-60, 1997.
[35] Hasim K.A., Kefal A.: Isogeometric static analysis of laminated plates with curvilinear fibers based on Refined Zigzag Theory. Composite Structures, 256: 113097, 2021.
[36] Wimmer H., Celigoj Chr., Timmers R.: Bending and Buckling of Shear-elastic Angle-ply Laminated Plates using Enhanced Refined Zigzag Theory. 14th International Conference on Computational Structures Technology, Montpellier, 2022.
[37] Erhart T., Brandner R., Schickhofer G., Frangi A.: Rolling Shear of some European Timber Species with Focus on Cross Laminated Timber (CLT): Test

Configuration and Parameter Study. INTER Proceedings, Meeting 48, Paper 48-6-1, 2015.
[38] Aicher S., Dill-Langer G.: Basic Considerations to Rolling Shear Modulus in Wooden Boards. Otto - Graf-Journal 11:157-165, 2000.

https://doi.org/10.52202/069179-0334